AGU PUBLICATIONS

JGR

Journal of Geophysical Research: Earth Surface

RESEARCH ARTICLE
10.1002/2017JF004214

Key Points:
- Stream discharge from the Tanana Flats Basin decreased 44% in April
- Snow cover area, snowpack water equivalent, and snowmelt decreased in spring
- Timings of snowmelt onset and ending have shifted by 2 (earlier) and 5 (later) days per decade, respectively

Supporting Information:
- Supporting Information S1

Correspondence to:
Q. Zhuang,
qzhuang@purdue.edu

Citation:
Liao, C., & Zhuang, Q. (2017). Quantifying the role of snowmelt in stream discharge in an Alaskan watershed: An analysis using a spatially distributed surface hydrology model. *Journal of Geophysical Research: Earth Surface*, *122*, 2183–2195. https://doi.org/10.1002/2017JF004214

Received 13 JAN 2017
Accepted 18 SEP 2017
Accepted article online 11 OCT 2017
Published online 13 NOV 2017

Quantifying the Role of Snowmelt in Stream Discharge in an Alaskan Watershed: An Analysis Using a Spatially Distributed Surface Hydrology Model

Chang Liao[1] **and Qianlai Zhuang**[1,2]

[1]Department of Earth, Atmospheric, and Planetary Sciences, Purdue University, West Lafayette, IN, USA, [2]Department of Agronomy, Purdue University, West Lafayette, IN, USA

Abstract This study uses a spatially distributed surface hydrology model to investigate the role of snowmelt in stream discharge for the Tanana Flats Basin in interior Alaska. The Parameter ESTimation code is used to calibrate the model with observed stream discharge data. The model was further evaluated using remote sensing-based snow cover product and in situ snowpack water equivalent (SWE) observations. A 36 year (1980–2015) U.S. Geological Survey Precipitation-Runoff Modeling System simulation shows (1) the monthly stream discharge from the Tanana Flats Basin in April decreased by 44%; (2) snow cover area at high altitudes (above 2000 m) decreased in summer, both SWE and snowmelt also decreased significantly, especially in spring; (3) the timings of snowmelt onset and ending shifted by 2 (earlier) and 5 (later) days per decade, respectively; and (4) snowmelt accounts for 40% of the annual stream discharge. This study provides a quantitative tool to investigating hydrological systems considering the impacts of snow dynamics in cold regions. This study also suggests that future warming will further decrease snow coverage, advance snow melting time, and hereafter change the stream discharge dynamics in the Arctic.

1. Introduction

The effects of global warming on the cryosphere are most visibly manifested on the snow cover and mountain glaciers. In northern high latitudes, the increase in near surface air temperature is almost twice as large as the global average (Hartmann et al., 2013). Arctic and subarctic hydrology systems will experience significant changes under the warming conditions (Kane, 1997; Vaughan et al., 2013). Recent studies have indicated that freshwater discharge into the Arctic Oceans has already increased due to snow and glacier melt (Arendt et al., 2002; Hill et al., 2015).

Although no consistent long-term trends in stream discharge were observed for global major rivers, stream discharge in spring has been increasing resulting from earlier snowmelt in northern high latitudes (Hartmann et al., 2013; Semmens & Ramage, 2013; St Jacques & Sauchyn, 2009). In the United States, stream discharge from Alaska contributes approximately 36% to the national total annual streamflow and 7 of the 20 largest rivers are located in Alaska (Bowersox, 2002; Krammer, 1990).

In northern high latitudes, snow dynamics play an important role in surface hydrology. While most studies have focused on snow metrics, only a few have quantified the relationship between snow dynamics and stream discharge. For example, many studies have suggested that changes in snow accumulation and ablation have changed the seasonal pattern of streamflow (Semmens & Ramage, 2013; Stone et al., 2002). For snow metrics, studies have suggested that snow cover, which plays a special role in surface energy balance, has undergone a significant reduction in recent decades in northern high latitudes (Brown & Robinson, 2011; Male & Granger, 1981; Stieglitz et al., 2003). To predict the spatial distribution and magnitude of future warming, it is imperative to improve our estimates of snow cover dynamics. Snowpack water equivalent (SWE), the liquid water that would be released upon complete melting, also has drawn much attention. Many studies have investigated SWE dynamics based on in situ observations or passive microwave remote sensing approaches (Mote et al., 2005). However, only a few of them were conducted in Alaska and they generally have relatively coarse spatial resolutions (Dozier et al., 2016; Foster et al., 2005). Snowmelt is also of great importance because it is essentially the most important water source for snowmelt-fed catchment and it accounts for most variations in stream discharge. In recent decades, many studies have suggested that the spatial

distribution and timing of snowmelt in Arctic and subarctic are changing (Semmens & Ramage, 2013; Stone et al., 2002). While most studies used in situ observations or remote sensing approaches, only a few used modeling approaches to quantify the snowmelt dynamics. In recent decades, modeling work of snow dynamics has drawn much attention and energy balance-based methods are more favored when high-quality climate and surface elevation data are available (Hock, 2005; Marks et al., 1999; Tarboton et al., 1994; Woo & Thorne, 2006).

To date, many attempts have been made to predict snowmelt-derived streamflow for efficient water resource management (Christiansen et al., 2011; Ferguson, 1999). However, only a few have used fully distributed approach in northern high latitudes (Fang et al., 2010; Levesque et al., 2008). In this study, we used a fully spatially distributed watershed model to investigate the snowmelt-streamflow relationship in an Alaskan watershed. Specifically, we used the U.S. Geological Survey (USGS) Precipitation-Runoff Modeling System (PRMS) to build our model (Leavesley et al., 1995; Markstrom et al., 2015). The calibrated model was evaluated with a set of observed stream discharge, in situ snowpack water equivalent data, and remote sensing snow cover area product. Finally, we applied the model to investigate the snowmelt-streamflow relationship. The major objectives of this study are to estimate and analyze the streamflow in an interior Alaskan watershed (16,000 km^2) and to quantify the role of snowmelt in streamflow in an Arctic hydrological system.

2. Study Area, Data, and Methods

2.1. Description of Study Area and Data

The Tanana Flats Basin (TFB), located in the interior Alaska near Fairbanks, drains an area of approximately 16,000 km^2. This basin is a typical snowmelt-fed catchment with extreme relief from the Mount Hayes in the eastern Alaska Range. Surface elevation decreases from about 4.0 km at Mount Hayes to around 120.0 m at the Tanana Flats in less than 50.0 km (Figure 1). In the southern part, the eastern Alaska Range forms the southern barrier of the glacier outwash. In the central part, the Tanana Flats occupies the alluvial fan. Only a few well-developed stream channels including the Clear Creek and Wood River run through the flats prior to joining the Tanana River. In the northern part, the Tanana River, which is the largest tributary of the Yukon River, runs from east near Big Delta to west near Nenana. Both surface water and groundwater near Fairbanks have been studied intensively for decades (Anderson, 1970; Viereck et al., 1993; Williams, 1965). Ecosystem of the Tanana Flats has also drawn much attention with emphasis on permafrost degradation (Jorgenson et al., 2001; Osterkamp et al., 2000; Racine & Walters, 1994; Seaton, 2002).

Glaciers near the Alaska Range cover up to 1% of the basin based on the World Glacier Inventory data (Figure 1) (WGMS and NSIDC, 1999). Recent studies have suggested that volumes of these glaciers are decreasing due to the changing climate (Arendt et al., 2002; Hill et al., 2015). Seasonal snowmelt is the major freshwater resource for most stream channels throughout the year. This region also lies within discontinuous permafrost zones under current climate. Approximately 60% of the basin is underlain by permafrost (Geophysical Institute Permafrost Lab, 2011). Earlier studies have also indicated that groundwater discharges to the land surface through permafrost-free zones at the Tanana Flats (Liao & Zhuang, 2017).

To conduct model simulations, a list of data set was prepared. Details of these data sets are listed in Table 1.

2.2. Model Description

PRMS is a spatially distributed and process-based modeling system to quantify the impacts of climate and land use on streamflow and watershed hydrology (Leavesley et al., 1983; Markstrom et al., 2015). For decades, it has been used extensively to investigate watershed-scale response to climate change (Battaglin et al., 2011; Christiansen et al., 2011; Risley et al., 2011). To date, most studies have used PRMS in temperate regions but few in northern high latitudes. In our study, we used the latest version PRMS-IV. We selected several modules including snow and stream flow routing modules to setup the PRMS model, and we output stream discharge and snow metrics for analyses (Figure 2).

In PRMS, a watershed is discretized into a network of hydrological response units (HRU) and each HRU contains a series of "reservoirs." Hydrological modules and algorithms including canopy interception, snow accumulation, and ablation are used to estimate the water stored or exchanged among these reservoirs (Markstrom et al., 2015).

The snow module in PRMS uses the water and energy-balance method to simulate the snow dynamics including snow cover area (SCA), snowpack water equivalent (SWE), and snowmelt. Energy balance is calculated

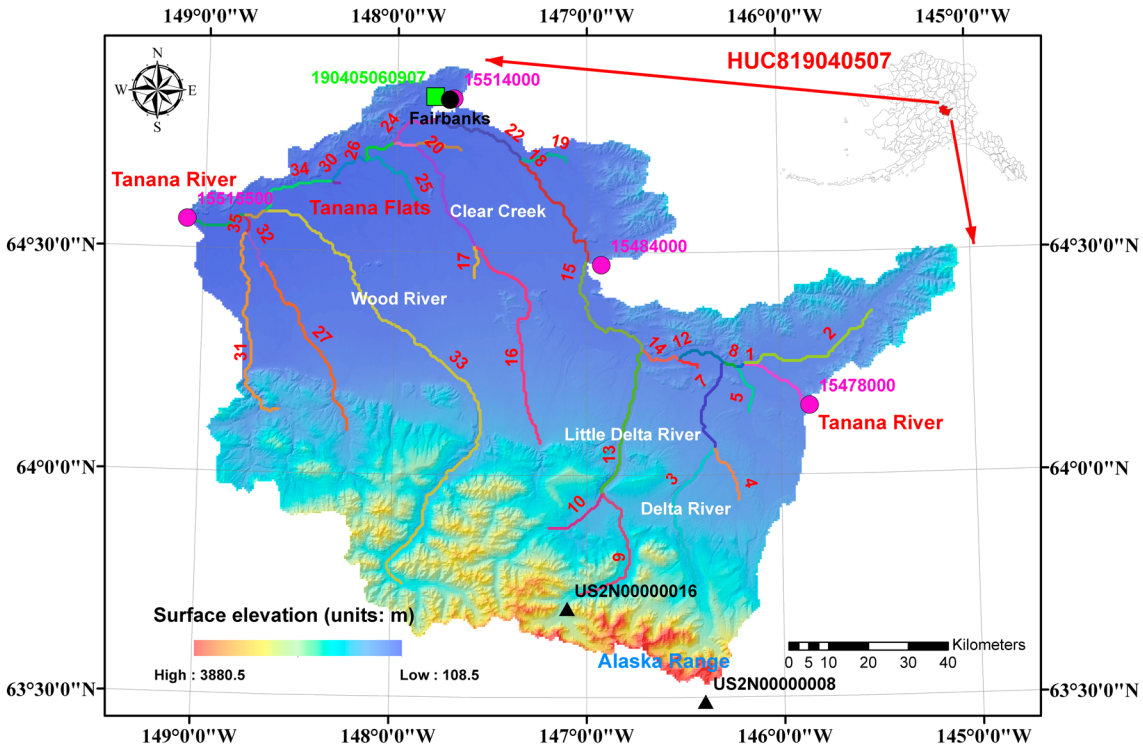

Figure 1. The spatial location and hydrological networks of the Tanana Flats Basin (TFB). The red-filled polygon in the upper right features the spatial location and extent of the Tanana Flats Basin in interior Alaska. HUC819040507 is the hydrologic unit codes (HUC) from the U.S. Geological Survey (USGS) Watershed Boundary Data Set. Black triangles are the locations of permanent glaciers from the World Glacier Inventory (WGI) data. Colored line features with numbered indices are the stream segments from watershed delineation. The Tanana River is represented by a series of connected stream segments. Segments 1, 18, and 24 receive inflow from upstream basins. Pink dots are the USGS gage stations (Table 2). Green square is the Snow Telemetry (SNOTEL) site. Black dot is the city of Fairbanks, Alaska.

at a half-day time step (day and night). Incoming shortwave/longwave and outgoing longwave radiations are calculated as

$$\text{Shortwave\_net}_{\text{hru}} = \text{Shortwave}_{\text{hru}} \times (1 - \text{albedo}) \times \text{trcf} \tag{1}$$

$$\text{Longwave}_{\text{hru}} = 5.67 \times 10^{-8} \times T^4 \tag{2}$$

$$\text{Longwave\_net}_{\text{hru}} = \text{Canopy\_den} \times \text{Longwave}_{\text{hru}} + (1 - \text{Canopy\_den}) \times \text{emis} \tag{3}$$

Table 1
List of Data Set Used

Data	Spatial resolution	Temporal resolution	Source	Description
Climate data	In situ	Daily	Global Historical Climatology Network (GHCN) (Menne et al., 2012)	Inputs for ANUSPLIN package
Digital elevation model	60 m	Time invariant	National Elevation Data set (Gesch et al., 2002)	Resampled to 500 m
Glacier data	In situ	Time invariant	World Glacier Inventory (WGMS and NSIDC, 1999)	
Hydrological data	In situ/polygon based	Daily	National Hydrography Data set/Watershed Boundary Data set and National Water Information System (U.S. Geological Survey, 2013)	Watershed delineation and stream discharge
Land use and land cover change data	30 m	Time invariant	National Land Cover Database (Fry et al., 2011)	Resampled to 500 m
Snow Telemetry data	In situ	Daily	Natural Resources Conservation Service's National Water and Climate center (Center & Data, 2016)	
Snow cover data	500 m	Daily	Moderate-resolution Imaging Spectroradiometer (MODIS) (Hall et al., 2006)	Cloud-free based on MODIS corrected reflectance images
Soil data	Polygon-based	Time invariant	Soil Survey Geographic Database (data sets) (Soil Survey Staff, 2015)	Polygon converted to raster

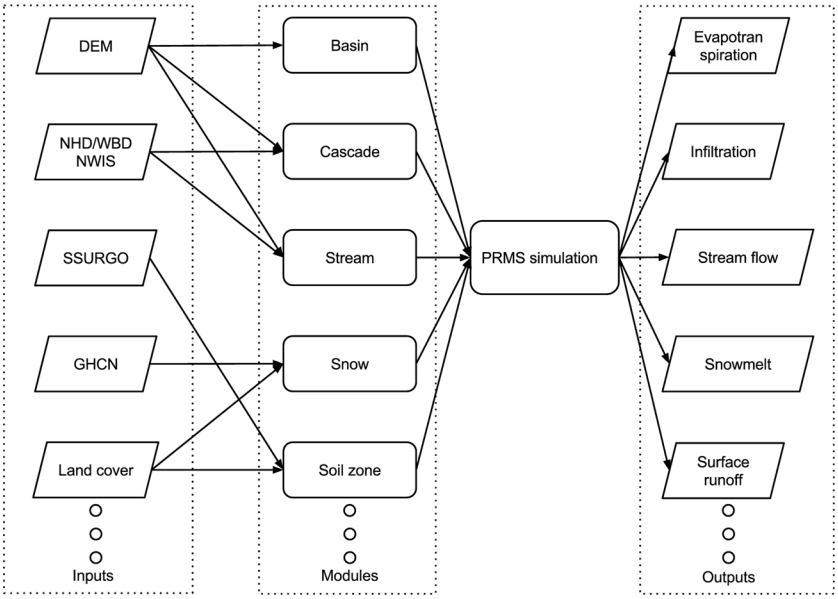

Figure 2. Data flow in the PRMS-IV model simulation. Details of data set are listed in Table 1. Modules used in PRMS-IV simulation include snow and stream flow routing modules. Details of these modules can be found in the PRMS-IV user guide (Markstrom et al., 2015). Model outputs include streamflow, snow cover area (SCA), and snowpack water equivalent (SWE).

where $\text{Shortwave\_net}_{hru}$ is the net shortwave radiation through vegetation canopy (units: J m^{-2} d^{-1}); Shortwave_{hru} is the effective shortwave radiation considering topography and climate (units: J m^{-2} d^{-1}); albedo is surface albedo (units: fraction); trcf is vegetative transmission coefficient (units: fraction); Longwave_{hru} is incoming longwave radiation (units: J m^{-2} d^{-1}); T is atmosphere temperature (units: Kelvin); $\text{Longwave\_net}_{hru}$ is net longwave radiation (units: J m^{-2} d^{-1}); Canopy_den is canopy density (units: fraction); and emis is the longwave emission from land cover (units: J m^{-2} d^{-1}). Sensible heat flux and latent heat flux are calculated based on precipitation and snowpack temperatures.

PRMS-IV also explicitly considers heat added by precipitation in forms of rain and snow (Markstrom et al., 2015).

Snowpack is conceptualized as two layers: (1) a surface layer with temperature controlled by near surface atmosphere conditions and (2) a bottom layer with temperature controlled by both heat exchange and previous snowpack conditions. Snowmelt is calculated when positive heat is applied to the snowpack as

$$\text{Snowmelt}_{hru} = \frac{\text{Heat}_{hru}}{C_{ice}} \times \text{SCA} \tag{4}$$

where Snowmelt_{hru} is the meltwater from snow and ice ablation (units: mm m^{-2} d^{-1}); Heat_{hru} is the heat added to the snow layer (units: J m^{-2} d^{-1}); C_{ice} is specific heat of ice (units: J kg^{-1} K^{-1}); and SCA is snow cover area (units: fraction). After each time step, snowpack properties including albedo, temperature, and SCA are updated. Details of these equations and terms can be found in the PRMS-IV user guide (Markstrom et al., 2015).

Special attention has been paid to elevation effects because snow dynamics are usually elevation dependent (Bell & Moore, 1999; Molotch et al., 2005; Winstral et al., 2002). Specifically, we divided the study area into several elevation bands and conducted analyses on both basin and elevation band levels.

Because PRMS does not explicitly distinguish glacier from snowpack, glacier is simply treated as snowpack with much larger thickness (Markstrom et al., 2015). In our study, initial thicknesses of glaciers were defined using the World Glacier Inventory (WGI) data (WGMS and NSIDC, 1999). Because the spatial coverage of glaciers is less than 1% in our study area, we speculate that the impact of this assumption should not be significant. As a result, we used the term snowmelt to represent meltwater from both snowpack and glacier unless otherwise stated.

Table 2
List of U.S. Geological Survey Gage Stations Used

Site ID	Datum of gage	Name
15478000	293.5 m above NGVD29	Southeast Fairbanks Census Area County, Alaska
15484000	192.6 m above NGVD29	Salcha River Near Salchaket, Alaska
15514000	130.5 m above NAVD88	Chena River at Fairbanks, Alaska
15515500	103.1 m above NGVD29	Yukon-Koyukuk Census Area County, Alaska

The grid-based approach was used to discretize the spatial domain. We used the System for Automated Geoscientific Analyses (SAGA GIS) and Arc Hydro tool to delineate the watershed and hydrological networks (Esri Water Resources Team, 2011; Olaya, 2004). Input data for Arc Hydro Tool includes digital elevation model (DEM) and 1:1,000,000-scale (medium resolution) flow line features. The following steps were carried out sequentially: (1) "burn" the NHD flowline through DEM reconditioning (Hellweger & Maidmentm, 1997), (2) fill the depressions in DEM, (3) calculate the flow direction and accumulation, and (4) define the drainage line and subbasin.

The whole basin is discretized into a matrix of HRUs. The horizontal resolution of each HRU is 500.0 m × 500.0 m. A total of 37 stream segments containing 1,570 stream reaches were delineated (Figure 1). We used the term stream to represent all stream channels including rivers and creeks unless otherwise stated. The cascade module was used to route surface and subsurface water flow between adjacent HRUs. We used the USGS Cascade Routing Tool to prepare the cascade parameters based on DEM and hydrological networks (Henson et al., 2013).

To provide spatially explicit climate data for model simulation, we interpolated the in situ GHCN data to the spatial domain using the ANUSPLIN package (Table 1). ANUSPLIN package uses thin plate smoothing spine surface fitting technique to interpolate spatial data set and has been widely used to process climate data (Hutchinson & Xu, 2013). In the end, daily climate data (maximum/minimum temperature and precipitation) at a 500.0 m spatial resolution were produced.

Because this basin receives streamflow from upstream, the observed stream discharge from four USGS gage stations were used. Three of them were used as model inputs, and the remaining one at the basin outlet (Site ID: 15515500) was used for model calibration and evaluation (Figure 1). Details of the gage stations used are listed in Table 2.

We used seasonal Mann-Kendall test to conduct all the time series trend analyses for stream discharge and snow metrics. We used the TIMESAT code to approximate the timings of snowmelt onset and ending. The TIMESAT code is a software package that uses several filters and smooth functions (e.g., adaptive Savitzky-Golay filter or least squares fitted asymmetric Gaussian) to extract seasonality information from time series remote sensing data (Eklundh & Jönsson, 2015). It has been widely used on various types of data (Olofsson & Eklundh, 2007). In our study, we applied TIMESAT to time series basin-averaged simulated snowmelt to estimate the timings of snowmelt onset and ending.

2.3. Model Calibration and Evaluation

The model-independent Parameter ESTimation and uncertainty analysis package (PEST) was used to automate our PRMS model calibration (Doherty et al., 1994). In PEST, the cost function is defined as

$$\Phi = [c - c_0 - J(b - b_0)]_t \times Q \times [c - c_0 - J(b - b_0)] \quad (5)$$

where c is the system simulated vector; c_0 is the "linearized" system simulated vector; J is the Jacobian matrix of the linearization function M that maps n-dimensional parameter space into m-dimensional observation space; b is the system parameter vector; and b_0 is the corresponding system parameter vector using M. To minimize the cost function, the linearized system parameter vector b_0 is updated through iterations until Φ is reduced to certain criteria. To improve calibration efficiency, we used the Message Passing Interface version of PEST, BeoPEST, to conduct parameter estimation.

To reduce the total number of parameters, the spatial domain is divided into several zones, within which parameters are assumed constancy. These zones are defined using land use and land cover, vegetation, and soil types. Special attention has been paid to topography effects since snow parameters are elevation

Table 3
Estimated Values of PRMS Model Parameters From BeoPEST Calibration

Module	Parameter	Description	Initial value	Calibrated value	Units
climateflow	tmax_allrain	Maximum temperature when precipitation is assumed to be rain	38.0	40.2	Fahrenheit
	tmax_allsnow	Maximum temperature when precipitation is assumed to snow	32.0	35.8	Fahrenheit
ddsolrad	ppt_rad_adj	Minimum precipitation for precipitation adjustment	0.02	0.014	inches
	radmax	Maximum fraction of potential solar radiation that reach ground	0.8	0.8	fraction
	radj_sppt	Precipitation adjustment factor for solar radiation in summer	0.44	0.1	fraction
	radj_wppt	Precipitation adjustment factor for solar radiation in winter	0.5	0.1	fraction
intcp	snow_intcp	Snow interception storage capacity	0.1	0.01	inches
	wrain_intcp	Winter rain interception storage capacity	0.1	0.04	inches
	srain_intcp	summer rain interception storage capacity	0.1	0.52	inches
	covden_sum	Summer vegetation density	0.5	0.39	fraction
	covden_win	Winter vegetation density	0.5	0.87	fraction
potet	transp_tmax	Temperature index to determine the start of transpiration	500.0	499.0	Fahrenheit
	jh_coef	Air temperature coefficient used in Jensen-Haise equation	0.014	0.005	fraction
	jh_coef_hru	Air temperature coefficient used in Jensen-Haise equation	13.0	13.1	per degree per Fahrenheit
snowcomp	albset_rna	Fraction of rain fraction above which snow albedo is not reset during snow accumulation	0.8	0.66	fraction
	albset_rnm	Fraction of rain fraction above which snow albedo is not reset during snow melt	0.6	0.87	fraction
	albset_sna	Minimum snow to reset snow albedo during snow accumulation	0.05	0.23	inches
	albset_snm	Minimum snow to reset snow albedo during snow accumulation	0.2	0.5	inches
	cecn_coef	Convection condensation energy coefficient	5.0	4.9	calories per degree
	potet_sublim	Fraction of potential evapotranspiration from snow sublimation	0.5	0.1	fraction
	settle_const	Snowpack settlement time constant	0.1	0.37	fraction
	snarea_thresh	Maximum snowpack water equivalent below which snow cover area curve is used	60.0	59.0	inches
	rad_trncf	Transmission coefficient of shortwave radiation through winter canopy	0.5	0.1	fraction
soilzone	pref_flow_den	Fraction of preferential flow in soil zone	0.2	0.5	fraction
	soil_moist_max	Maximum soil moisture	5.0	6.0	inches
	soil_rechr_max	Maximum storage for soil recharge zone	1.5	1.0	inches
srunoff	carea_max	Maximum possible area contributing to surface runoff	0.6	0.97	fraction
	snowinfil_max	Maximum snow infiltration	2.0	2.0	inches per day

Note. Details of modules and parameters can be found in the PRMS-IV user guide (Markstrom et al., 2015).

dependent (Bell & Moore, 1999; Winstral et al., 2002). We also conducted a sensitivity analysis to identify the most sensitive parameters. Overall, a total of 28 parameters in 7 PRMS modules were calibrated (Table 3).

We ran our PRMS model for 36 years from 1980 to 2015. To remove the effects from arbitrary initial conditions, the first 10 years served as a spin-up period. We calibrated the model using daily streamflow observations from year 1990 to 2000 at the basin outlet (Site ID: 15515500). The parameter calibration results are listed in Table 3. Details of modules and parameters can be found in the PRMS-IV user guide. We evaluated the model performance using the remaining data from 2001 to 2015. Statistics including Percent Bias (PBIAS) and Nash-Sutcliffe efficiency (NSE) were used to compare the observed and simulated discharge rates (Moriasi et al., 2007). During the calibration period, PBIAS and NSE are 11.6% and 0.88, respectively. During the evaluation period, PBIAS and NSE are 7.3% and 0.90 (Table 4). Time series plot of the simulated discharge rates has shown that our estimates capture both interannual and intraannual variability with a Pearson's coefficient (r) of 0.95 (two-sided P value less than 0.01).

We further evaluated our model with in situ snowpack water equivalent data at a SNOTEL site located near Fairbanks (Figure 1). Comparison between the observed and simulated SWE has shown that our model performed well. PBIAS is less than 15% during both calibration and evaluation periods. NSE is higher than 0.7 (Table 5). Similar to streamflow, simulated SWE captured the interannual and intraannual variability

Table 4
Statistical Comparison of Observed and Simulated Annual Stream Discharge at the Basin Outlet for the Calibration (1990–2000) and Evaluation (2001–2015) Periods

	Observed ($m^3\ d^{-1}$)	Simulated ($m^3\ d^{-1}$)	PBIAS(%)	NSE	R
Calibration period	8.1×10^{12}	7.1×10^{12}	10.2	0.89	0.95
Evaluation period	8.2×10^{12}	7.6×10^{12}	7.3	0.9	0.90

Table 5
Statistical Comparison of Observed and Simulated Mean Snowpack Water Equivalent (SWE) at the SNOTEL Site for the Calibration (1990–2000) and Evaluation (2001–2015) Periods

	Observed (mm)	Simulated (mm)	PBIAS(%)	NSE	R
Calibration period	57.3	48.2	14	0.72	0.9
Evaluation period	51.3	49.3	3.8	0.79	0.9

with a Pearson's coefficient (r) of 0.9 (two sided P value less than 0.01) (Figures S1 and S2 in the supporting information). However, SWE might have been underestimated due to input data quality. We also evaluated the simulated snowmelt indirectly because direct measurements are unavailable. By definition, changes in SWE, specifically, the decrease in SWE, can be viewed as a result of snowmelt and snow sublimation. Therefore, we estimated the "observed" snowmelt using observed SWE and simulated snow sublimation. Time series observed and simulated snowmelt have shown that our estimates are reasonable. But snowmelt might have been underestimated similar to SWE, and great uncertainty still remains. We further compared the simulated SCA with MODIS snow cover product (MOD10A1) from 24 February 2000 to present. In MOD10A1, snow cover is characterized by the fractional snow cover (FSC), which has the same definition with SCA (Hall et al., 2006). MOD10A1 has been evaluated and used extensively (Brubaker et al., 2005). Because MOD10A1 is often affected by cloud, we only compare SCA with FSC in nearly cloud-free days based on MODIS-corrected reflectance images (Hall & Riggs, 2007; Vermote et al., 2011). Comparison between SCA and FSC has shown that our estimates are reasonable. For example, on 23 April 2015, the spatial patterns and magnitudes of SCA and FSC are very close (Figures 3 and S3). Also on 14 June 2015, both SCA and FSC have captured the spatial distribution of snow cover due to glaciers near the Alaska Range.

3. Results

3.1. Stream Discharge Dynamics

Both observed and simulated discharge at the basin outlet have shown a strong seasonality over the 26 years. The average discharge rates are 2.0×10^8 m^3 d^{-1} and 1.8×10^7 m^3 d^{-1} in summer and winter, respectively (Figure 4). No significant trend was detected in time series annual discharge (two-sided P value larger than 0.1). Actual discharge from the Tanana Flats Basin was estimated by subtracting upstream inflow from the discharge at the outlet (Figure 1). Because the average discharge from the Tanana River at Big Delta is much larger than the actual discharge from TFB and those from the Salcha River and Chena River, on an annual basis, the Tanana River at Big Delta contributes approximately 70% to the total discharge and the TFB contributes 10%. Similar to stream discharge at the basin outlet, no significant trend was detected in time series annual actual discharge from TFB and the decrease is only 1% based on linear regression analysis. However, a significant decreasing trend was detected for monthly total discharge in April (two-sided P value less than 0.05), within which the total discharge has decreased by 44% from 8.0×10^6 m^3 d^{-1} to 4.3×10^6 m^3 d^{-1}. We further analyzed the daily actual discharge by month for the calibration and evaluation periods. Our analyses have confirmed that daily discharge in April has decreased substantially whereas increased in July. In other months, the differences vary slightly (Figure 5). Within the Tanana Flats Basin, simulated discharge from tributaries of the Tanana River varies significantly. Among them, Clear Creek usually has the highest discharge rate (5.0×10^6 m^3 d^{-1}) in summer. As a result, on an annual basis, Clear Creek (64.4%), followed by Wood River (9.8%) and Little Delta River (7.8%), contributes the largest amount of discharge into the Tanana River. However, their contributions change drastically due to snowmelt onset and the Wood River usually overruns the Clear Creek in discharge in spring.

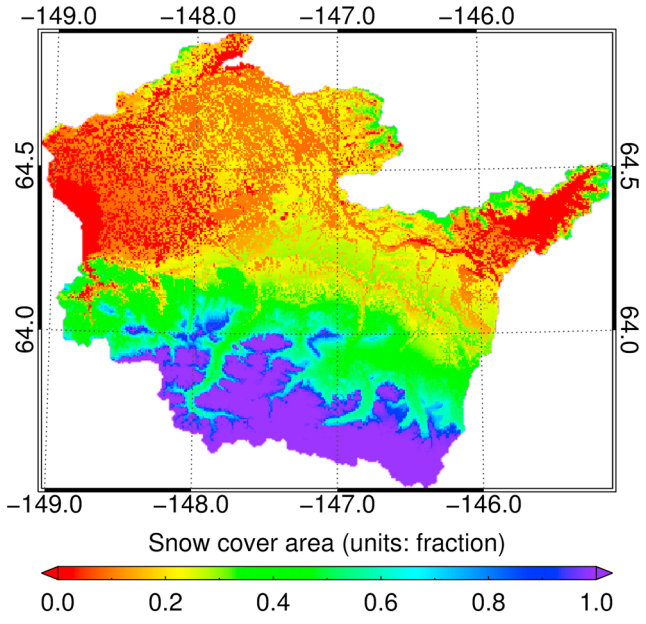

Figure 3. The spatial distribution of simulated PRMS snow cover area (SCA) on 23 April 2015 (units: fraction).

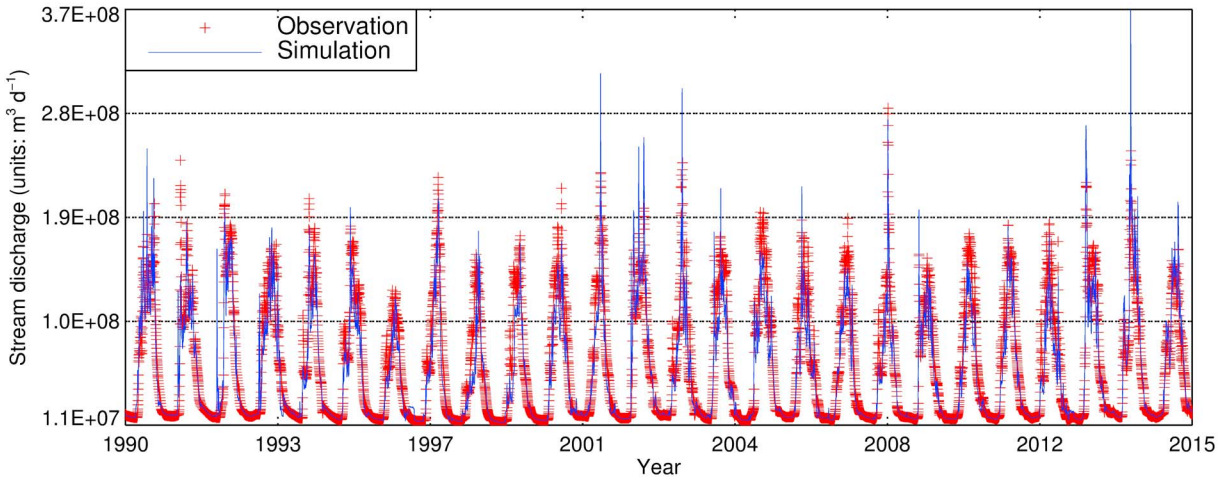

Figure 4. Time series observed and simulated stream discharge rates at the basin outlet from year 1990 to 2015 (units: $m^3\ d^{-1}$).

3.2. Snow Dynamics

3.2.1. Snow Cover Area Dynamics

In PRMS, snow cover is characterized by the snow cover area (SCA), which is defined as the percentage of area covered by snow for each HRU. The simulated SCA has shown a significant spatial-temporal variability. First, simulated SCA has shown a strong seasonality with the largest variations in April and October. It often reaches the highest spatial coverage and magnitude in winter whereas the lowest in late summer. No significant trend in time series basin-averaged SCA was detected. However, for elevation bands higher than 2,000 m, significant decreasing trends were detected in June and July (two-sided *P* value of 0.01). Second, spatial and temporal variations of the simulated SCA are always interrelated with each other. In lowlands, SCA usually drops drastically within 1 week in spring due to snowmelt onset, whereas in regions near the Alaska Range, SCA does not decrease until late summer. For example, on 23 April 2015, the simulated SCA has shown that more than 50% of TFB (mostly in lowlands) has completely lost snow cover (Figure 3). Whereas in high altitudes, SCA barely decreased since winter. In late summer, most regions will lose snow cover whereas regions near the Alaska Range may be still covered by glaciers.

3.2.2. Snowpack Water Equivalent Dynamics

The simulated snowpack water equivalent (SWE) has shown that most variations in SWE are associated with variations in SCA. This is because in PRMS SWE is closely coupled with SCA. First, the simulated SWE is also affected by surface elevation. For example, on 1 May 2015, the spatial distribution of simulated SWE is highly correlated with surface elevation and the average SWE in high altitudes (more than 70 mm) is much larger

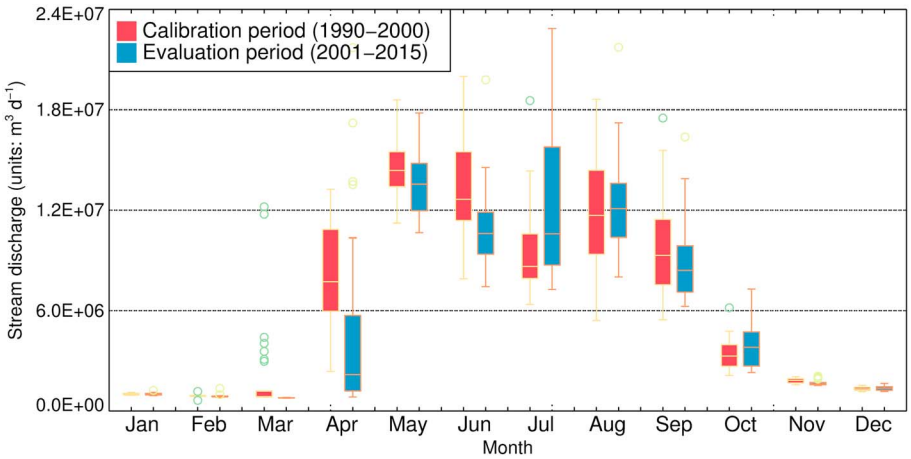

Figure 5. Basin total daily stream discharge by month for the calibration (1990–2000) and evaluation (2001–2015) periods (units: $m^3\ d^{-1}$).

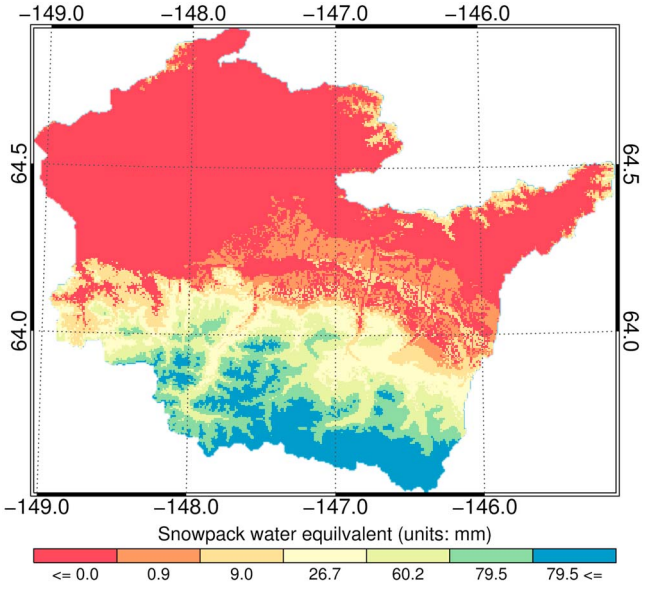

Figure 6. The spatial distribution of simulated PRMS snowpack water equivalent (SWE) on 1 May 2015 (units: mm).

than that in lowlands (less than 1 mm) (Figure 6). Second, because snowpack accumulation and ablation are cumulative processes, the intraannual variability of the simulated SWE is smoother than that of SCA. Unlike SCA, significant decreasing trends were detected in the basin-averaged SWE for several months (two-sided *P* value of 0.05). During the evaluation period (2001–2015), the basin-average SWE in January (54.4 mm) and February (65.8 mm) is only 65% of those (82.3 mm and 100.5 mm, respectively) in the calibration period (1990–2000) (Figure 7). For elevation bands higher than 1500 m, the decreasing trends are even more significant. Due to the presence of glaciers, the simulated SWE near the Alaska Range is persistently the highest throughout the simulation. In other regions, the simulated SWE has shown a strong seasonality. In general, SWE always increases to its maximum until snowmelt forms and then decreases to its minimum in late summer. Time series analyses of mean SWE at different elevation bands by month have further elucidated the relationship between SWE dynamics and elevation. During the snowpack ablation process (spring to summer), because increase in temperature always starts from lowlands, decrease in SWE also starts from the corresponding elevation band, that is, 0–500 m. As temperature increase expands spatially, SWE at higher elevations bands starts (e.g., 1,500–2,000 m) to decrease. As a result, the decrease in SWE gradually shifts from lowlands to high altitudes (Figure S4). During the snowpack accumulation process (autumn to winter), regardless of elevation band, SWE increases simultaneously. However, the accumulation rate is still correlated with elevation. As a result, the maximum SWE at elevation band 1,500–2,000 m (~140 mm) is much higher than that at elevation band 0–500 m (~75 mm).

3.2.3. Snowmelt Dynamics

The simulated snowmelt has shown a significant spatial-temporal variability, which is affected by the spatial-temporal variability of SWE. A significant decreasing trend in basin-averaged snowmelt was detected in several months including March and April (two-sided *P* value of 0.01) (Figure 8). The spatial-temporal variability of snowmelt is controlled by temperature and snow availability. In general, when snow is abundant, temperature is the dominant factor. Whereas when temperature is above the melting point, snow availability becomes the dominant factor. Temperature increase always starts from lowlands and then shifts to high altitudes, so does snowmelt onset. For example, on 28 March 2015, the highest snowmelt rate was from elevation band 0–500 m (more than 4.5 mm) (Figure S5). Whereas on 28 April 2010, the highest snowmelt rate was overtaken by elevation band 1,500–2,000 m (more than 5.5 mm) (Figure 9). Time series analyses of mean snowmelt at different elevation bands by month have further revealed the transition of snowmelt onset and ending at different elevation bands. In April, snow melting mainly took place in lowlands. In May, the mean snowmelt

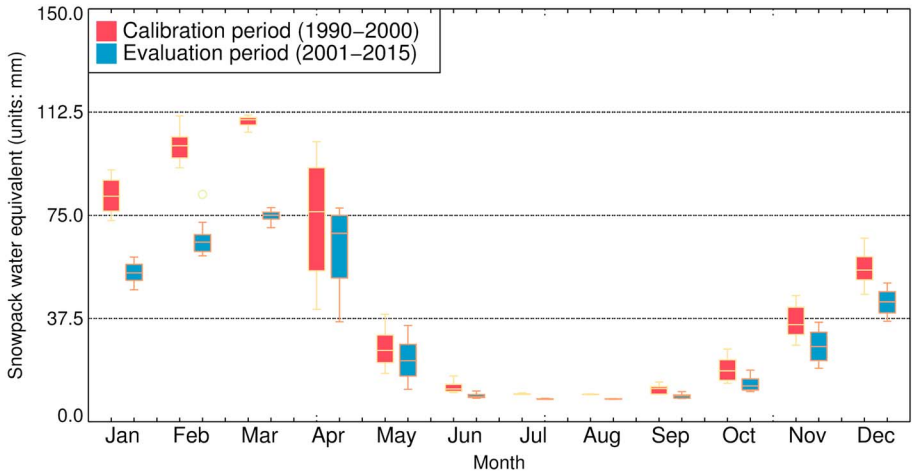

Figure 7. Basin-averaged daily snowpack water equivalent (SWE) by month for the calibration (1990–2000) and evaluation (2001–2015) periods (units: mm).

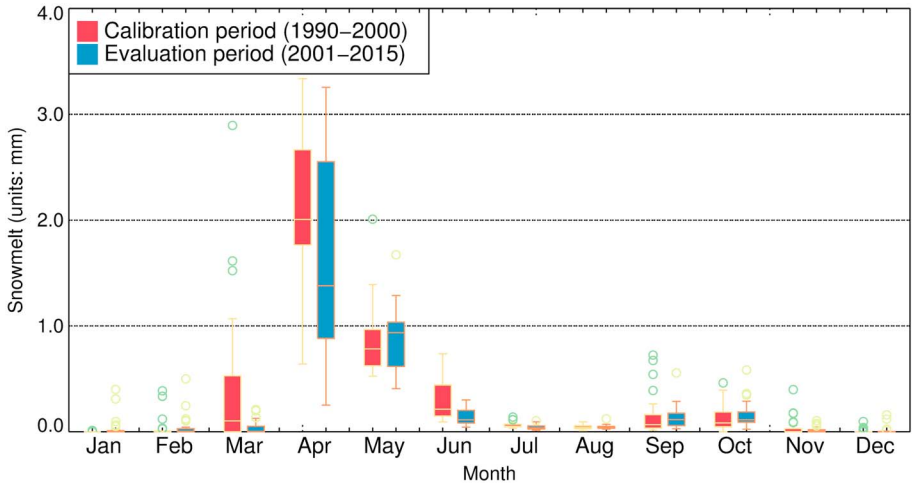

Figure 8. Basin-averaged daily snowmelt by month for the calibration (1990–2000) and evaluation (2001–2015) periods (units: mm).

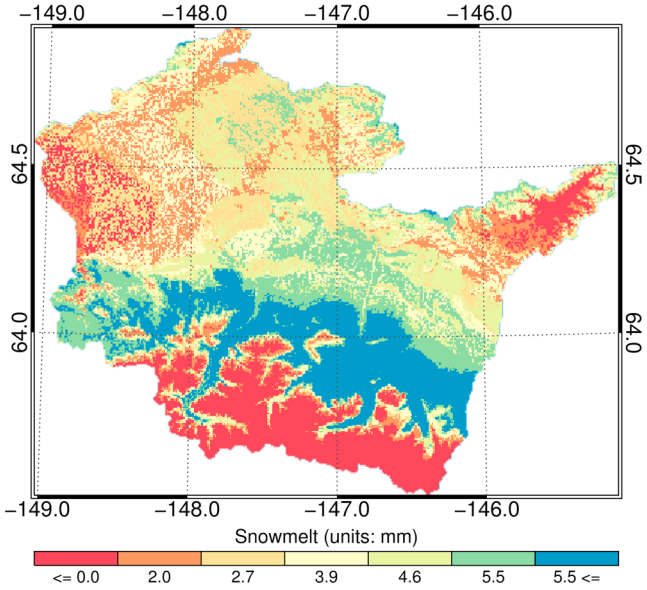

Figure 9. The spatial distributions of simulated snowmelt on 28 April 2015 (units: mm).

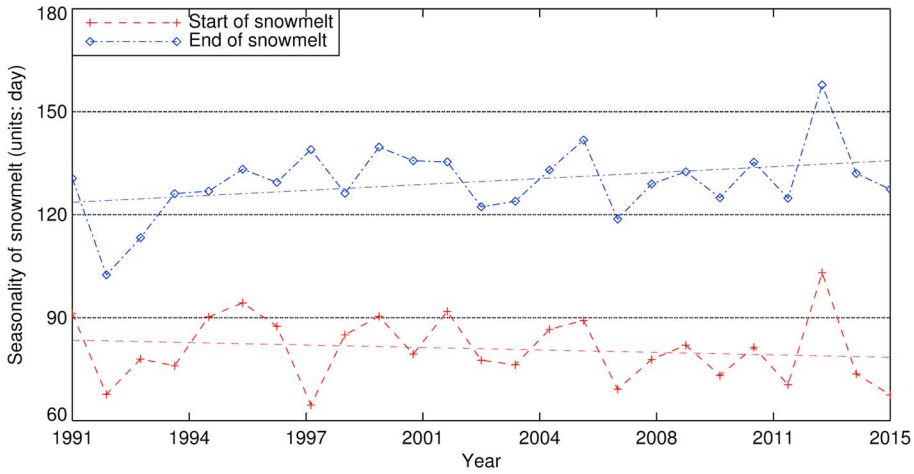

Figure 10. Timings of snowmelt onset and ending based on TIMESAT analysis from year 1991 to 2015. The red and blue lines are the days of snowmelt onset and ending, respectively.

rate in lowlands dropped to 1.0 mm and it climbed to over 2.5 mm at elevation band 1,500–2,000 m. In June, snowmelt in lowlands was negligible whereas it reached to 4.0 mm at elevation band 2,000–2,500 m (Figure S6). Near the Alaska Range, snowmelt rate was persistently the lowest due to extremely low temperature.

TIMESAT analysis on daily basin-averaged snowmelt rate has indicated that the timings of snowmelt onset and ending are changing. During the simulation period, the timing of snowmelt onset has shifted 2 days earlier per decade whereas the snowmelt ending has shifted 5 days later per decade (Figure 10). Due to shifted snowmelt onset and ending, the total duration of snow melting has increased by 7 days per decade.

4. Discussions

The simulated stream discharge has shown that even though the annual stream discharge from the Tanana Flats Basin has not changed much, the monthly stream discharge in April has decreased by 44% from 1990 to 2015, which implies snowmelt in spring is decreasing (Figure 5).

Our analyses on the simulated snow metrics have confirmed that snow dynamics are changing. First, even though no significant trend was detected in time series basin-averaged snow cover area (SCA), SCA at higher altitudes is potentially decreasing due to warming temperature.

Second, significant decreasing trends were detected in time series basin-averaged snowpack water equivalent (SWE) in several months, especially in January, February, and March (Figure 7). Because SWE holds the upper limit of potential snowmelt, decrease in total snowmelt is expected.

Third, the simulated snowmelt is decreasing in several months (i.e., March and April). This is mainly due to the decrease in SWE in precedent months (i.e., January and February). Moreover, the timings of snowmelt onset and ending have shifted. In early spring, the timing of snowmelt onset has shifted 2 days earlier per decade due to warming temperature. In late spring, because snowmelt gradually expands to higher altitudes than usual, the timing of snowmelt ending has also shifted 5 days later per decade. Our findings are consistent with other studies (Brown & Robinson, 2011; Semmens & Ramage, 2013; Stone et al., 2002; Tan et al., 2011).

Simulation results have shown that snowmelt dynamics play an important role in stream discharge. In spring, surface runoff is the key component that bridges snowmelt and stream discharge. On average, snowmelt accounts for 90% of the surface runoff. Because surface runoff accounts for more than 90% of the stream discharge, snowmelt essentially accounts for more than 80% of the stream discharge. In other seasons, snowmelt decreases substantially due to either low temperature or snow availability. However, meltwater ("old water") that infiltrates into the soil previously continues to feed stream discharge through subsurface flow and groundwater upwelling.

On an annual basis, the total snowmelt is 4.7×10^6 m^3 d^{-1}. About 10% of the snowmelt joins the surface runoff (1.4×10^6 m^3 d^{-1}) directly and the rest 90% infiltrates into the soil zone. Meanwhile, 20% of the total streamflow (7.1×10^6 m^3 d^{-1}) comes from the surface runoff. Subsurface flow (1.9×10^6 m^3 d^{-1}) and groundwater upwelling (3.8×10^6 m^3 d^{-1}) make up the rest of 27% and 53%, respectively. Therefore, subsurface flow and groundwater flow also play an important role in stream discharge dynamics, which is consistent with other studies (Liao & Zhuang, 2017; Woo, 2012).

Taken together, simulation results have shown that snowmelt accounts for 40% of the total stream discharge on an annual basis on average. Because snowmelt is partitioned into surface infiltration and runoff whereas stream discharge is composed of surface runoff, subsurface flow, and groundwater upwelling, snowmelt contributes to stream discharge through multiple pathways and its total contribution varies significantly with season.

5. Conclusions

Our spatially distributed hydrological model simulations have indicated that the annual stream discharge from the Tanana Flats Basin has only decreased by 1% from 1990 to 2015. However, the monthly stream discharge in April has decreased by 44% from 8.0×10^6 m^3 d^{-1} to 4.3×10^6 m^3 d^{-1} due to decrease in snowmelt.

Seasonal snowmelt plays a major role in the rapid changes in stream discharge. In spring, a significant decreasing trend was detected in snowmelt, which explains the decrease in stream discharge. In other seasons,

snowmelt continues to contribute to stream discharge through subsurface flow and groundwater flow. On an annual basis, snowmelt accounts for 40% of the total stream discharge on average. The timings of snowmelt onset and ending have shifted by 2 (earlier) and 5 (later) days per decade, respectively. As a result, the total snowmelt duration has increased by 7 days per decade.

Our simulations have demonstrated that the spatially distributed hydrological model performs well in the study area. As warming continues in the Arctic, we speculate that the seasonal pattern of stream discharge will be further affected by the changing snow dynamics. Our study also suggests that permafrost degradation and glacier dynamics play an important role in Arctic hydrological cycle. Thus, the enhanced three-dimensional modeling tool considering these processes shall be applicable for future Arctic hydrological studies.

Acknowledgments

This study is supported through projects funded to Qianlai Zhuang by the NASA Land Use and Land Cover Change program (NASA-NNX09AI26G), Department of Energy (DE-FG02-08ER64599), the NSF Division of Information and Intelligent Systems (NSF-1028291), and a project from the United States Geological Survey focusing on quantification of carbon and methane dynamics in Alaska. This research was supported in part through computational resources provided by Information Technology at Purdue, West Lafayette, Indiana. We gratefully thank the technical supports received from USGS PRMS team. We also thank the assistance from Willem Schreuder on model calibration. All data used in this study can be obtained through corresponding data sources. The data presented in this study will be deposited to our research laboratory website (www.purdue.edu/eaps/ebdl) to allow the public to access.

References

Anderson, G. S. (1970). Hydrologic reconnaissance of the Tanana basin (Tech. Rep.) Central Alaska: U.S. Geological Survey.

Arendt, A. A., Echelmeyer, K. A., Harrison, W. D., Lingle, C. S., & Valentine, V. B. (2002). Rapid wastage of Alaska glaciers and their contribution to rising sea level. *Science*, *297*(5580), 382–386.

Battaglin, W., Hay, L., & Steve, M. (2011). Simulating the potential effects of climate change in two Colorado basins and at two Colorado ski areas. *Earth Interactions*, *15*(22), 1–23.

Bell, V. A., & Moore, R. J. (1999). An elevation-dependent snowmelt model for upland Britain. *Hydrological Processes*, *13*(12–13), 1887–1903.

Bowersox, R. (2002). Hydrology of a glacial dominated system, Copper River, Alaska. In J. Mount, P. Moyle, & S. Yarnell (Eds.), *Glacial and periglacial processes as hydrogeomorphic and ecological drivers in high-latitude watersheds*. Davis, CA. Retrieved from https://watershed.ucdavis.edu/copper_river/backgBowersoxCopper.pdfround/data/

Brown, R. D., & Robinson, D. A. (2011). Northern Hemisphere spring snow cover variability and change over 1922–2010 including an assessment of uncertainty. *The Cryosphere*, *5*(1), 219–229.

Brubaker, K. L., Pinker, R. T., & Deviatova, E. (2005). Evaluation and comparison of MODIS and IMS snow-cover estimates for the continental United States using station data. *Journal of Hydrometeorology*, *6*(6), 1002–1017.

Center, N. S., & Data, I. (2016). All About Snow. National Snow and Ice Data Center. Accessed 06/02 2016. https://nsidc.org/cryosphere/snow. Boulder, CO: National Snow and Ice Data Center.

Christiansen, D. E., Markstrom, S. L., & Hay, L. E. (2011). Impacts of climate change on the growing season in the United States. *Earth Interactions*, *15*(33), 1–17.

Doherty, J., Brebber, L., & Whyte, P. (1994). PEST: Model-independent parameter estimation, Watermark Computing, Corinda, Australia.

Dozier, J., Bair, E. H., & Davis, R. E. (2016). Estimating the spatial distribution of snow water equivalent in the world's mountains. *Wiley Interdisciplinary Reviews: Water*, *3*(3), 461–474.

Eklundh, L., & Jönsson, P. (2015). TIMESAT: A software package for time-series processing and assessment of vegetation dynamics. *Remote Sensing Time Series* (pp. 141–158). Lund, Sweden: Springer.

Esri Water Resources Team (2011). Arc Hydro Tools - Tutorial. Redlands, CA: ESRI.

Fang, X., Pomeroy, J. W., Westbrook, C. J., Guo, X., Minke, A. G., & Brown, T. (2010). Prediction of snowmelt derived streamflow in a wetland dominated prairie basin. *Hydrology and Earth System Sciences*, *14*(6), 991–1006.

Ferguson, R. I. (1999). Snowmelt runoff models. *Progress in Physical Geography*, *23*(2), 205–227.

Foster, J. L., Sun, C., Walker, J. P., Kelly, R., Chang, A., Dong, J., & Powell, H. (2005). Quantifying the uncertainty in passive microwave snow water equivalent observations. *Remote Sensing of Environment*, *94*(2), 187–203.

Fry, J. A., Xian, G., Jin, S., Dewitz, J. A., Homer, C. G., Limin, Y., … Wickham, J. D. (2011). Completion of the 2006 national land cover database for the conterminous United States. *Photogrammetric Engineering and Remote Sensing*, *77*(9), 858–864.

Geophysical Institute Permafrost Lab (2011). GIPL1.3 simulated maximum active layer thickness (ALT) in meters averaged for particular decade for the entire Alaskan permafrost domain, NAD83, Alaska Albers Projection. Fairbanks, AK: University of Alaska, Fairbanks.

Gesch, D., Oimoen, M., Greenlee, S., Nelson, C., Steuck, M., & Tyler, D. (2002). The national elevation dataset. *Photogrammetric Engineering and Remote Sensing*, *68*(1), 5–32.

Hall, D. K., & Riggs, G. A. (2007). Accuracy assessment of the MODIS snow products. *Hydrological Processes*, *21*(12), 1534–1547.

Hall, D. K., Riggs, G. A., & Salomonson, V. V. (2006). *MODIS/Terra snow cover 8-day L3 global 500 m grid V005*. Boulder, CO: National Snow and Ice Data Center.

Hartmann, D. J. L., Klein Tank, A. M. G., Rusicucci, M., Alexander, L. V., Broenniman, B., Charabi, Y. A.-R., … Zhai, P. (2013). Observations: Atmosphere and surface. In *Climate change 2013: The physical science basis* (pp. 159–254). Contribution of Working Group I to the Fifth Assessment Report of the Intergovernmental Panel on Climate Change. Cambridge, UK and New York: Cambridge University Press.

Hellweger, F., & Maidmentm, D. (1997). AGREE-DEM surface reconditioning system. Retrieved from http://www.ce.utexas.edu/prof/maidment/gishydro/ferdi/research/agree/agree.html, last accessed 3 March 2005.

Henson, W. R., Medina, R. L., Mayers, C. J., Niswonger, R. G., & Regan, R. S. (2013). CRT–Cascade Routing Tool to define and visualize flow paths for grid-based watershed models, U.S. Department of the Interior, U.S. Geological Survey, Reston, VA.

Hill, D. F., Bruhis, N., Calos, S. E., Arendt, A., & Beamer, J. (2015). Spatial and temporal variability of freshwater discharge into the Gulf of Alaska. *Journal of Geophysical Research: Oceans*, *120*, 634–646. https://doi.org/10.1002/2014JC010395

Hock, R. (2005). Glacier melt: A review of processes and their modelling. *Progress in Physical Geography*, *29*(3), 362–391.

Hutchinson, M. F., & Xu, T. B. (2013). *ANUSPLIN version 4.4 user guide*. Canberra: Australian National University.

Jorgenson, M. T., Racine, C. H., Walters, J. C., & Osterkamp, T. E. (2001). Permafrost degradation and ecological changes associated with a warming climate in central Alaska. *Climatic Change*, *48*(4), 551–579.

Kane, D. L. (1997). The impact of hydrologic perturbations on Arctic ecosystems induced by climate change, *Global change and Arctic terrestrial ecosystems* (pp. 63–81). New York: Springer.

Krammer, J. C. (1990). Largest rivers in the United States. Reston, VA: U.S. Geological Survey. Retrieved from https://pubs.usgs.gov/of/1987/ofr87-242/

Leavesley, G. H., Lichty, R. W., Thoutman, B. M., & Saindon, L. G. (1983). *Precipitation-runoff modeling system user's manual*. Colorado: US Geological Survey Colorado.

Leavesley, G. H., Stannard, L. G., & Singh, V. P. (1995). The precipitation-runoff modeling system PRMS, *Computer models of watershed hydrology* (pp. 281–310). Highlands Ranch, CO: Water Resources Publications.
Levesque, E., Anctil, F., Van Griensven, A. N. N., & Beauchamp, N. (2008). Evaluation of streamflow simulation by SWAT model for two small watersheds under snowmelt and rainfall. *Hydrological Sciences Journal*, *53*(5), 961–976.
Liao, C., & Zhuang, Q. (2017). Quantifying the role of permafrost distribution in groundwater and surface water interactions using a three-dimensional hydrological model. *Arctic, Antarctic, and Alpine Research*, *49*(1), 81–100.
Male, D. H., & Granger, R. J. (1981). Snow surface energy exchange. *Water Resources Research*, *17*(3), 609–627.
Marks, D., Domingo, J., Susong, D., Link, T., & Garen, D. (1999). A spatially distributed energy balance snowmelt model for application in mountain basins. *Hydrological Processes*, *13*(12–13), 1935–1959.
Markstrom, S. L., Regan, R. S., Hay, L. E., Viger, R. J., Webb, R. M. T., Payn, R. A., & LaFontaine, J. H. (2015). PRMS-IV, the precipitation-runoff modeling system (version 4, Tech. Rep.). Reston, VA: U.S. Geological Survey.
Menne, M. J., Durre, I., Vose, R. S., Gleason, B. E., & Houston, T. G. (2012). An overview of the global historical climatology network-daily database. *Journal of Atmospheric and Oceanic Technology*, *29*(7), 897–910.
Molotch, N. P., Colee, M. T., Bales, R. C., & Dozier, J. (2005). Estimating the spatial distribution of snow water equivalent in an alpine basin using binary regression tree models: The impact of digital elevation data and independent variable selection. *Hydrological Processes*, *19*(7), 1459–1479.
Moriasi, D. N., Arnold, J. G., Van Liew, M. W., Bingner, R. L., Harmel, R. D., & Veith, T. L. (2007). Model evaluation guidelines for systematic quantification of accuracy in watershed simulations. *Transactions of the ASABE*, *50*(3), 885–900.
Mote, P. W., Hamlet, A. F., Clark, M. P., & Lettenmaier, D. P. (2005). Declining mountain snowpack in western North America. *Bulletin of the American Meteorological Society*, *86*(1), 39.
Olaya, V. (2004). *A gentle introduction to SAGA GIS* (p. 208). Gottingen, Germany: The SAGA User Group eV.
Olofsson, P., & Eklundh, L. (2007). Estimation of absorbed PAR across Scandinavia from satellite measurements. Part II: Modeling and evaluating the fractional absorption. *Remote Sensing of Environment*, *110*(2), 240–251.
Osterkamp, T. E., Viereck, L., Shur, Y., Jorgenson, M. T., Racine, C., Doyle, A., & Boone, R. D. (2000). Observations of thermokarst and its impact on boreal forests in Alaska, USA. *Arctic, Antarctic, and Alpine Research*, *32*, 303–315.
Racine, C. H., & Walters, J. C. (1994). Groundwater-discharge fens in the Tanana Lowlands, interior Alaska, USA. *Arctic and Alpine Research*, *26*(4), 418–426.
Risley, J., Moradkhani, H., Hay, L., & Markstrom, S. (2011). Statistical comparisons of watershed-scale response to climate change in selected basins across the United States. *Earth Interactions*, *15*(14), 1–26.
Seaton, T. C. (2002). Winter foraging ecology of moose in the Tanana flats and Alaska Range foothills (PhD thesis), University of Alaska Fairbanks.
Semmens, K. A., & Ramage, J. M. (2013). Recent changes in spring snowmelt timing in the Yukon River basin detected by passive microwave satellite data. *The Cryosphere*, *7*(3), 905–916.
Soil Survey Staff (2015). Natural Resources Conservation Service, United States Department of Agriculture. Web Soil Survey. Retrieved from http://websoilsurvey.nrcs.usda.gov/, accessed 06/02/2015
St Jacques, J.-M., & Sauchyn, D. J. (2009). Increasing winter baseflow and mean annual streamflow from possible permafrost thawing in the Northwest Territories Canada. *Geophysical Research Letters*, *36*, L01401. https://doi.org/10.1029/2008GL035822
Stieglitz, M., Déry, S. J., Romanovsky, V. E., & Osterkamp, T. E. (2003). The role of snow cover in the warming of Arctic permafrost. *Geophysical Research Letters*, *30*(13), 1721. https://doi.org/10.1029/2003GL017337
Stone, R. S., Dutton, E. G., Harris, J. M., & Longenecker, D. (2002). Earlier spring snowmelt in northern Alaska as an indicator of climate change. *Journal of Geophysical Research*, *107*(D10), 4089. https://doi.org/10.1029/2000JD000286
Tan, A., Adam, J. C., & Lettenmaier, D. P. (2011). Change in spring snowmelt timing in Eurasian Arctic rivers. *Journal of Geophysical Research*, *116*, D03101. https://10.1029/2010JD014337
Tarboton, D. G., Chowdhury, T. G., & Jackson, T. H. (1994). A spatially distributed energy balance snowmelt model (*Report, Paper 60*). Logan, UT: Utah State University. Retrieved from http://digitalcommons.usu.edu/water_rep/60
U.S. Geological Survey (2013). National hydrography geodatabase: The national map viewer available on the World Wide Web, accessed 2 June 2015, at url [http://viewer.nationalmap.gov/viewer/nhd.html?p=nhd].
Vaughan, D. G., Comiso, J. C., Allison, I., Carrasco, J., Kaser, G., Kwok, R., … Zhang, T. (2013). Observations: Cryosphere. In T. F. Stocker et al. (Eds.), *Climate change 2013: The physical science basis* (pp. 317–382), Contribution of Working Group I to the Fifth Assessment Report of the Intergovernmental Panel on Climate Change. Cambridge United Kingdom and New York, NY: Cambridge University Press. https://doi.org/10.1017/CBO9781107415324.012
Vermote, E. F., Kotchenova, S. Y., & Ray, J. P. (2011). MODIS surface reflectance user's guide, MODIS Land Surface Reflectance Science Computing Facility, version, 1. Greenbelt, MD.
Viereck, L. A., Dyrness, C. T., & Foote, M. J. (1993). An overview of the vegetation and soils of the floodplain ecosystems of the Tanana River, interior Alaska. *Canadian Journal of Forest Research*, *23*(5), 889–898.
WGMS and NSIDC (1999). World glacier inventory. Compiled and made available by the World Glacier Monitoring Service (Tech. Rep.) Boulder CO, USA: Zurich, Switzerland, and the National Snow and Ice Data Center. https://doi.org/10.7265/N5/NSIDC-WGI-2012-02
Williams, J. R. (1965). *Ground water in the permafrost regions of Alaska*. Washington, DC: U.S. Government Printing Office.
Winstral, A., Elder, K., & Davis, R. E. (2002). Spatial snow modeling of wind-redistributed snow using terrain-based parameters. *Journal of Hydrometeorology*, *3*(5), 524–538.
Woo, M., & Thorne, R. (2006). Snowmelt contribution to discharge from a large mountainous catchment in subarctic Canada. *Hydrological Processes*, *20*(10), 2129–2139.
Woo, M.-K. (2012). *Permafrost hydrology*. Berlin: Springer Science and Business Media.